Journal of Applied Polymer Science

Hexafunctional Poly(propylene glycol) Based Hydrogels for the Removal of Heavy Metal Ions

Sudan Zheng,[1] Jin Young Shin,[1] Song Yi Song,[1] Seong Jae Yu,[1] Hongsuk Suh,[2] Il Kim[1]

[1]BK21 PLUS Center for Advanced Chemical Technology, Department of Polymer Science and Engineering, Pusan National University, Pusan 609-735, South Korea

[2]Department of Chemistry and Chemistry Institute for Functional Materials, Pusan National University, Pusan 609-735, South Korea

Correspondence to: I. Kim (E-mail: ilkim@pusan.ac.kr)

ABSTRACT: Two types of degradable poly(propylene glycol) (PPG) hydrogels that are suitable for the absorption of heavy metals have been presented. The PPG-O-P(O)Cl_2 fragments obtained by treating hexafunctional PPG with phosphorous oxychloride ($POCl_3$) react with 1,3-propanediamine (PDA; **Gel-1**) or PDA together with 1,2-ethanedithiol (**Gel-2**), to yield cross-linked and water-swellable hydrogels in a one-pot method. This protocol for the fabrication of PPG hydrogels exhibits promising advantages over prior methods including a short reaction time, mass-production, easy separation, and high yield. A series of heavy metal ions were employed to test the adsorptive properties of the hydrogels. **Gel-2** shows better adsorption capacity than **Gel-1** for all the metal ions and the metal ions adsorption efficiency of the two types of hydrogels is in the order of Fe(III) > Pb(II) > Cd(II) > Zn(II) > Cu(II) > Ni(II) > Co(II) > Hg(II). The amounts of metal ions adsorbed increases with metal ion concentration and hydrogel dosage, but decreases with temperature. © 2014 Wiley Periodicals, Inc. J. Appl. Polym. Sci. **2014**, *131*, 40610.

KEYWORDS: adsorption; crosslinking; gels; separation techniques; swelling

Received 5 November 2013; accepted 14 February 2014

DOI: 10.1002/app.40610

INTRODUCTION

Hydrogels are three-dimensional, cross-linked hydrophilic polymer networks with porous structures and are capable of absorbing large amounts of liquids, and thus they also present a high degree of flexibility in structural design.[1] As a result of their unique properties including stimulus response, osmosis, elasticity, and sorption, hydrogels have been used in superabsorbent materials, drug delivery systems, wastewater decontamination processes, catalyst carriers, smart materials, and tissue engineering.[2–4] Recently, hydrogels have attracted attention for the removal of heavy-metal pollutants, like Ni^{2+}, Cu^{2+}, Zn^{2+}, and Cd^{2+} ions that threaten to human health and the environment, from water bodies because of their ability of incorporating different chelation groups into the polymeric networks.

Whereas the conventional adsorbents such as activated carbon, clay, and ion-exchange resins can adsorb such species into pores or onto a large surface area, hydrogels form complexes with metal ions through the functional groups, such as hydroxyl, amine, carboxylic acid, ester, amide, and sulfonic acid groups, in their network structures, and a slight swelling of the three-dimensional networks of hydrogels is beneficial to reduce mass-transfer resistance. Thus, synthetic polymer hydrogels can control the diffusion process and bind chemical species through their polar functional groups. These functional groups existing in cross-linked polymeric materials can be manipulated easily for specific applications, such as functioning as complex agents for heavy metal ion removal from wastewater. In this sense, polymer hydrogels can be considered novel, highly responsive, and high-capacity adsorbent materials for the removal of heavy metal ions from wastewater. Even though hydrogels possess relatively high adsorption capacities and rates, some obstacles should be solved for practical application, such as the poor structural integrity leading to their fragility in water and poor metal binding capacity in variable external water conditions. In addition, high price and non-degradability have limited their application because of the growing public attention focused on energy sources, resources, and the environment.

Among the family of synthetic hydrogels, poly(ethylene glycol) (PEG) based hydrogels have attracted considerable interest, which are preferable for multipurpose biomedicine applications, as PEGs are biocompatible[5,6] and avoid an immune response with blood and cellular proteins.[7] A number of methods have been developed for the preparation of cross-linked PEG, such as

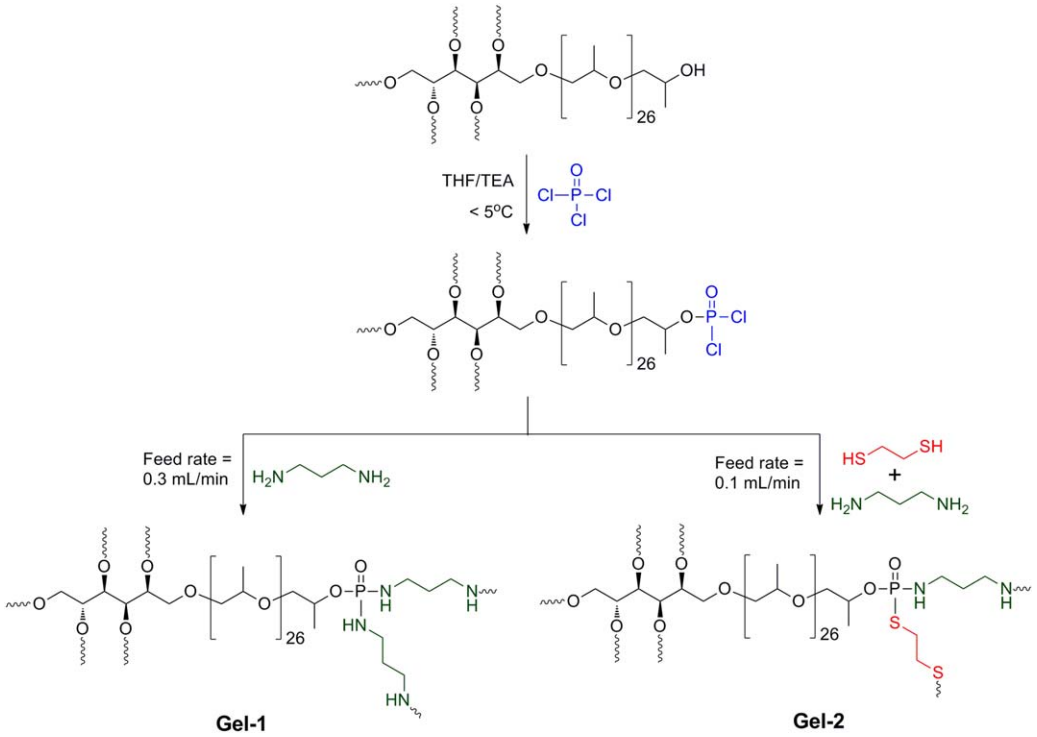

Scheme 1. One-pot synthesis of PPG hydrogels by using sorbitol-initiated hexafunctional PPG, phosphoryl oxychloride, 1,3-propanediamine and 1,3-ethanedithiol. [Color figure can be viewed in the online issue, which is available at wileyonlinelibrary.com.]

click chemistry[8] and radicals initiation generated from thermal energy,[9] redox reactions,[10] or the photocleavage of initiator molecules.[11–13] However, most of the methods for the preparation of PEG hydrogel require multistep reactions and work-up procedures potentially limiting the easy tuning of scaffold architectures and the mechanical strength of hydrogels, so that created hydrogels that are generally lacking structural integrity. In addition the reports on the hydrogels fabricated by poly(propylene glycol) (PPG) are scarce.

Variety of methods including chemical precipitation, reverse osmosis, membrane systems, solvent extraction, adsorption, electrolytic processes, ion exchange processes, and biological methods were employed for heavy metal ions removal from industrial wastewater. Among these methods, adsorption is one of the most economically favorable and it is technically an easy method.[14–16] However, most of the absorbents are difficult to fabricate and economically expensive, and have disadvantages such as low adsorption capacity and nondegradability. Thus, considerable attention has been focused on the development of economic and degradable adsorbents derived from low-cost materials.

In this article, guided by a previous report on the fabrication of a biocompatible gel with phosphorous oxychloride ($POCl_3$) as a cross-linker of diethylaminoethyl-pullulan,[17] we have investigated the synthesis and characterization of a new series of cross-linked water-swellable PPG hydrogels with degradable cross-linking spots composed of phosphorester, phosphoramide, and phosphorthiester bonds (Scheme 1). The preparation of the hydrogels is straightforward using condensation crosslinking reactions in a one-pot process with short reaction time. Note that in addition to these bonds, the hydrogels bear variety of functional groups such as ether, amine, thiol, and hydroxyl groups, which can be utilized to chelate various heavy metal ions. For the enhancement of structural integrity of hydrogel the sorbitol-initiated hexafunctional PPG was chosen and two types of hydrogels (i.e., **Gel-1** and **Gel-2**, without and with sulfur atoms, respectively) were designed in order to compare their capacities towards the adsorption of various heavy metal ions [i.e., Fe(III), Cu(II), Ni(II), Co(II), Zn(II), Cd(II), Hg(II), and Pb(II)]. The experimental parameters, such as metal ion concentration, adsorption temperature and time, which could influence the adsorption efficiency, were also investigated in detail. The newly invented protocol for the fabrication of PPG hydrogels exhibits promising advantages over prior methods including a short reaction time, mass-production, easy separation, and high yield. The metal ions adsorption efficiency of the two types of hydrogels is in the order of Fe(III) > Pb(II) > Cd(II) > Zn(II) > Cu(II) > Ni(II) > Co(II) > Hg(II).

EXPERIMENTAL

Materials

Hexafunctional PPG ($M_n = 9600$) was dried in a vacuum oven at 100°C prior to use. Tetrahydrofuran (THF) was distilled before use. Triethylamine (TEA; 99%), $POCl_3$ (99%), 1,3-propanediamine (PDA; 98%), 1,3-ethanedithiol (EDT; 90%), ferric(III) ammonium citrate (98%), cobalt(II) chloride (97%), nickel(II) nitrate hexahydrate (98%), copper (II) nitrate hemipentahydrate (99.99%), zinc(II) nitrate hexahydrate (98%), cadmium(II) chloride (99%), lead(II) chloride (99%), and

mercury(II) chloride (99.5%) were purchased from Sigma Aldrich and used without further purification.

Synthesis of Hydrogels

Synthetic reactions were performed in a one-pot process. Briefly, for the synthesis of **Gel-1** (Scheme 1), PPG (20 g) was dissolved in 80 mL of THF, followed by the addition of TEA (20 mL) under vigorous stirring in a 250-mL round flask equipped with a mechanical stirrer. After 30 min, $POCl_3$ (10 mL) was injected at a constant rate of 0.5 mL/min and the reaction temperature was held below 5°C for 1 h. Then, PDA (20 mL) was injected at a constant rate of 0.3 mL/min to form the hydrogel. Because of its insolubility in THF, the hydrogel was easily obtained by direct removal of the solvent and placed in deionized (DI) water for 2 days, changing the water every 4 h to remove any unreacted reagents and impurities. **Gel-2** (Scheme 1) was synthesized using a similar process to that described above except that EDT (10 mL) was additionally added after the addition of PDA.

Characterization

The gel content was determined on the cured films by measuring the weight loss after 48 h extraction with water at 100°C according to the standard test method ASTM D2765-84. Prior to spectroscopic analyses, the hydrogel samples were dried under vacuum overnight until they reached a constant weight. The dried hydrogel was pressed into a powder, mixed with 10 times as much KBr powder, and then compressed into a pellet for characterization by FT-IR spectroscopy[18] (Shimadzu IR Prestige-21spectrophotometer) in the region of 400–4000 cm^{-1}. Solid state ^{31}P NMR spectra were obtained on a Varian Unity 200 MHz spectrometer, operating at a ^{31}P NMR frequency of 202.5 MHz and samples were packed into 4 mm zirconia rotors. NMR spectra were obtained with the scanning number of 300, spinning rate of 11 kHz, and relaxation delays of 30 s.

For the morphological studies, the hydrogel samples were first immersed in ultrapure water for at least 48 h to reach equilibrium. Then, the swollen hydrogel samples were freeze-dried for 24 h. The surface morphologies of the freeze-dried gels were investigated by scanning electron microscope (SEM, Hitachi S-3000H, Japan). Specimens were coated with gold for 30 s using SEM coating equipment.[19] The thermo-behavior of the hydrogel samples was determined using a TA TGA 2050 instrument, which monitors the weight change of heated samples. The experimental procedure involved setting the sample inside an aluminum foil followed by heating the samples under flowing nitrogen (99.999% purity, 100 mL min^{-1}) from 20°C to 700°C at a rate of 10°C/min.

As a method of testing the mechanical property of hydrogels, storage modulus (G′) and loss modulus (G″) were measured with a rotational rheometer (Physical Rheometers UDS200, Anton Paar Ltd.) in parallel plate geometry with a 20 mm diameter acrylic upper plate, at 40°C, a frequency of 1–100 rad s^{-1}, and a constant strain (2%). For the measurement, the dried hydrogel discs with 20 mm diameter and 1 mm thickness were subjected to swelling in 10-m*M* phosphate buffer saline (PBS; pH 7.4) at 40°C. The water from the hydrogel surface was carefully blotted before measurement. G′ was measured at regular intervals until the hydrogels had insufficient physical integrity to handle.

Swelling Ratio Measurements

The swelling ratios (SRs) of **Gel-1** and **Gel-2** were obtained gravimetrically. Dried **Gel-1** and **Gel-2** samples (0.06 g) were immersed in DI water at 25°C for a designated time period. The samples were carefully removed and the residual water was separated using filter paper. The SRs of the samples at certain intervals of time were measured according to the following equation[20]:

$$SR = \frac{W_2 - W_1}{W_1} \quad (1)$$

where W_1 is the mass of dried hydrogel and W_2 is the mass of swollen hydrogel at a certain time.

Metal Ion Adsorption Measurement

Dried hydrogels were immersed in metal ion solutions dissolved in distilled water for 24 h. The residual solutions were analyzed using an ICP-MS and a UV-vis spectrophotometer (UV-1650PC, Shimadzu, Japan) to determine the ion concentration of the remaining solution. The amount of adsorbed metal ions was indirectly calculated as follows:

$$Q_e = \frac{(C_0 - C_t) \times V}{m} \quad (2)$$

where Q_e is the adsorption capacity of the hydrogel for metal ions at the adsorption equilibrium, C_0 is the initial metal ion concentration (g/L), C_t is the metal ion concentration after t (h) of adsorption by the hydrogel, V is the solution volume (mL), and m is the mass of the dried hydrogel (g).

Computational Studies for Gel-1 and Gel-2 Fragments

The quantum chemical calculations were carried out by density functional theory (DFT) as it usually gives realistic geometries, relative energies, electrostatic potential (ESP) fitted charges, and so on for analogous **Gel-1** and **Gel-2** fragments. All calculations were performed with the DMol^3 DFT code[21] as implemented in the Accelrys Materials Studio® 6.0 (http://www.accelrys.com/) on a personal computer (Intel® CoreTM i7 CPU at 3.47 GHz, 24.00 gigabytes ram) operated with Microsoft Windows 7 Ultimate K. The nonlocal generalized gradient approximation functional by Perdew-Burke-Ernzerhof[22] was used for all geometry optimizations. DMol^3 utilizes a basis set of numeric atomic functions, which are exact solutions to the Kohn–Sham equations for the atom.[23] In this study, a polarized split valence basis set, termed double numeric polarized basis set was used. All geometry optimizations employed highly efficient delocalized internal coordinates.[24]

RESULTS AND DISCUSSION

Synthesis and Characterization of the Hydrogels

As a means of developing new methods for the preparation of structurally integral hydrogels avoiding independent multistep reactions and tedious work-up procedures, one-pot method using hexafunctional PPG was employed. Simply treating PPG with $POCl_3$ at low temperature yielded PPG–$POCl_2$ fragments (Scheme 1). Reaction of these fragments with PDA or PDA together with EDT in THF gave **Gel-1** or **Gel-2**, respectively, which were directly separable from THF. **Gel-1** contains ether,

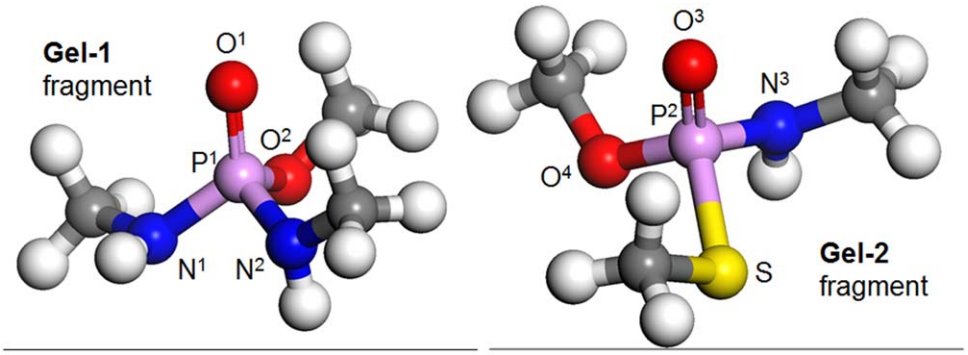

Length (Å)	Angle (deg)	ESP charge	Length (Å)	Angle (deg)	ESP charge
P^1-O^1 1.492	$O^1P^1N^1$ 122.326	P^1 1.086	P^2-O^3 1.489	$O^3P^2N^3$ 113.794	P^2 0.747
P^1-O^2 1.636	$O^1P^1O^2$ 113.033	O^1 -0.691	P^2-O^4 1.626	$O^3P^2O^4$ 116.366	O^3 -0.493
P^1-N^1 1.678	$O^1P^1N^2$ 111.603	O^2 -0.306	P^2-N^3 1.675	O^3P^2S 114.875	O^4 -0.390
P^1-N^2 1.672	$N^1P^1N^2$ 100.322	N^1 -0.766	P^2-S 2.101	SP^2N^3 105.782	N^3 -0.436
	$N^2P^1O^2$ 110.876	N^2 -0.667		$N^3P^2O^4$ 102.368	S -0.190
	$N^1P^1O^2$ 97.293			SP^2O^4 102.096	

Figure 1. Optimized geometry, geometric data, and ESP charges of **Gel-1** and **Gel-2** fragments obtained by B3LYP/6-31G** method. [Color figure can be viewed in the online issue, which is available at wileyonlinelibrary.com.]

phosphorester, and phosphoramide groups on the backbone and amine and hydroxyl groups on the periphery, whereas **Gel-2** contains phosphorthiester groups in addition to those in **Gel-1** on the backbone and thiol groups together with amine and hydroxyl groups on the periphery.

In order to get further insights on the structural characteristics of **Gel-1** and **Gel-2**, DFT calculations were performed on the expected backbone fragments. Computational studies of these new compounds were made by DFT (B3LYP) and force field methods (MM2). Different quantum-chemical parameters like ESP charges were calculated by B3LYP/6–31G** methods. Figure 1 shows the geometry optimized structures of the fragments consisting of phosporester and pohophoramide (**Gel-1**) and phosporester, pohophoramide and phosphorthiester (**Gel-2**) together with bond length, bond angle, and ESP-fitted charge data. As expected bond length (2.101 Å) between P^2 and S atoms is much longer than other bonds. Comparing angles of O^1–P^1–O^2 (122.326°) with O^3–P^2–O^4 (116.366°), and O^1–P^1–N^1 (122.326°) with O^3–P^2–N^3 (113.794°), corresponding angles in **Gel-2** are smaller than those in **Gel-2** because of the presence of sulfur atom in **Gel-2**. These data have significance for the structural formation of hydrogel networks and adsorption capacity for interaction with the metal ions and chemical and physical properties of the hydrogel. Figure 1 contains atomic charges, calculated by the ESP procedure, which might participate in hydrogen bonding with water molecules and in forming intermolecular interactions with metal ions added. Phosphorous atom in **Gel-1** show much bigger electropositive charge than that in **Gel-2** fragment. N1 atom shows the biggest electronegative charge in **Gel-1**, whereas O^3 atom represents the biggest electronegative charge in **Gel-2**. Of all the atoms showing electronegativity, sulfur atom shows the smallest electronegativity (−0.190).

In order to use the hydrogels for the adsorption of metal ions from wastewater, the structure especially the network of the hydrogel that generally affects the adsorption capability are very important. Hence, the surface morphologies of the **Gel-1** and **Gel-2** were analyzed by SEM, as shown in Figure 2; the results show that both types of hydrogels comprise three-dimensional network structures. **Gel-2**, bearing additional phosporthiester groups, has a less compact network structure than **Gel-1**, most probably because of the relatively bigger P–S length. In general, both hydrogels exhibit an even, sponge-like structure, and no phase separation is evident in the SEM images, which implies that a complete network structure is formed. The structure is connective and microporous; this should impart a faster diffusion rate because the effective diffusion distance can be controlled via the average distance between neighboring pores.[25] Suzuki and Hirasa[26] synthesized bulky poly(methyl vinyl ether) hydrogels, which had fine porous structures. The swelling of these sponge-like gels is orders of magnitude faster than that of any other responsive gels of comparable dimension; the pore sizes also affect the swelling properties of hydrogels. Based on the microporous structure, the synthesized hydrogels are expected to have good adsorption properties.[27]

In addition the hydrogel exhibits good structural integrity and flexibility in the water-swollen state (Figure 3), which is more advantageous for use as adsorbent. Excellent shape retention and high swellability of such hydrogel may enhance the capacity for metal ions absorption.

Spectroscopic Analysis of the Hydrogels

The FT-IR spectra of PPG, **Gel-1**, **Gel-2**, and **Gel-2** adsorbing Fe(III) (**Gel-2**-Fe), Cu(II) (**Gel-2**-Cu), Ni(II) (**Gel-2**-Ni), Co(II) (**Gel-2**-Co), Hg(II) (**Gel-2**-Hg), and Pb(II) (**Gel-2**-Pb) ions are

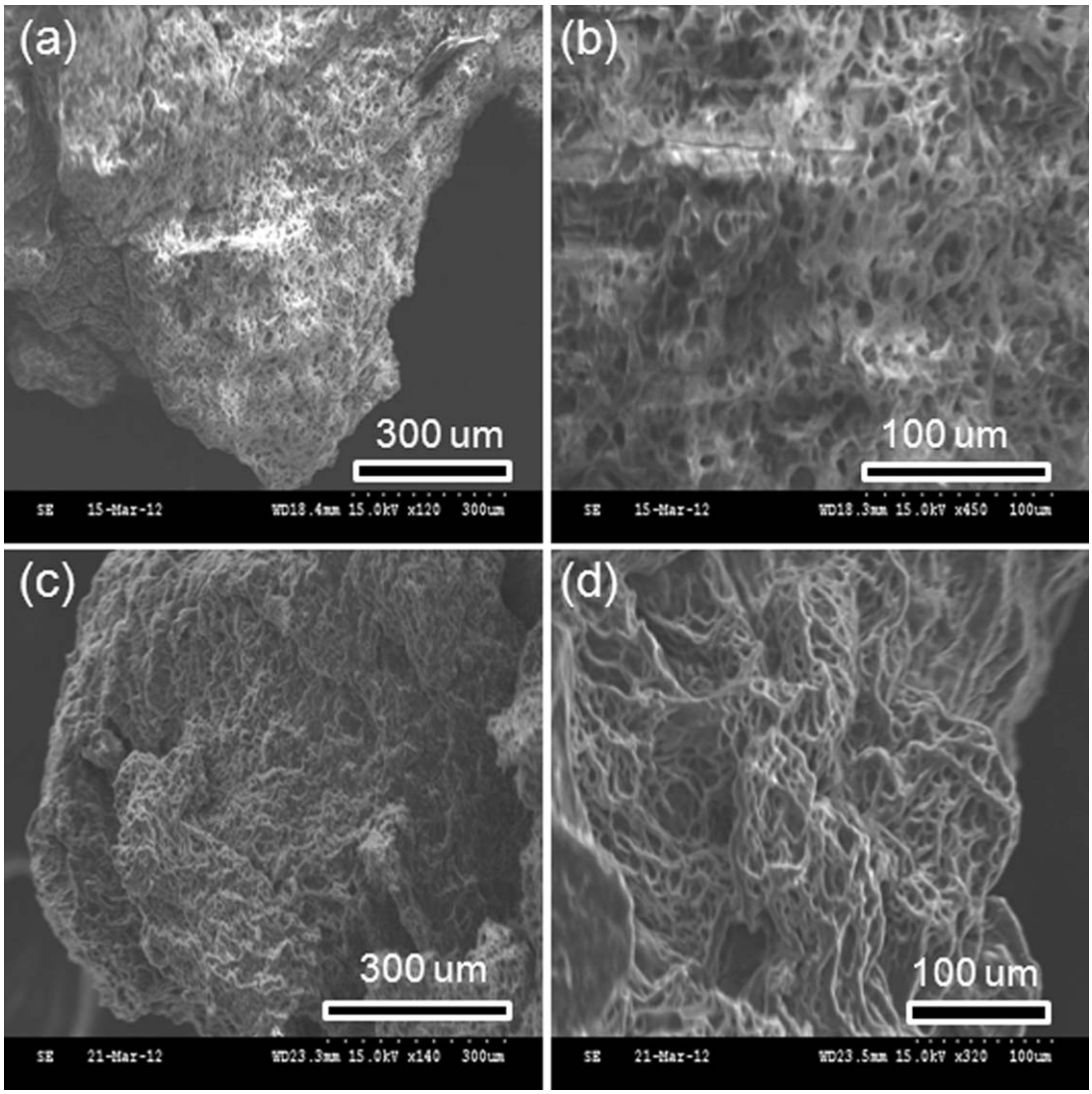

Figure 2. SEM images of (a, b) **Gel-1** and (c, d) **Gel-2**. The images were taken after freeze-drying of the gels.

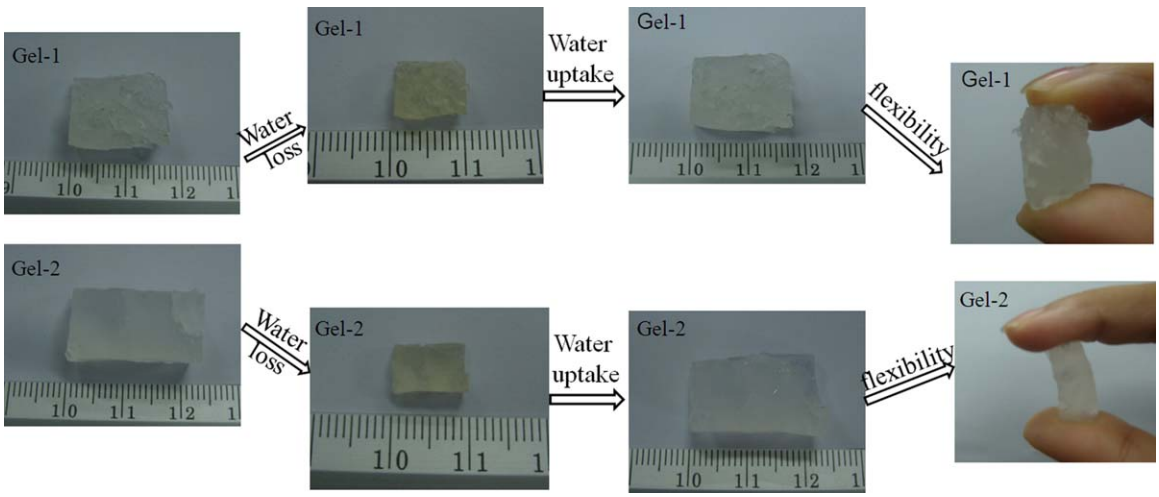

Figure 3. Photographic images of the hydrogels (**Gel-1** and **Gel-2**) with the promising properties. [Color figure can be viewed in the online issue, which is available at wileyonlinelibrary.com.]

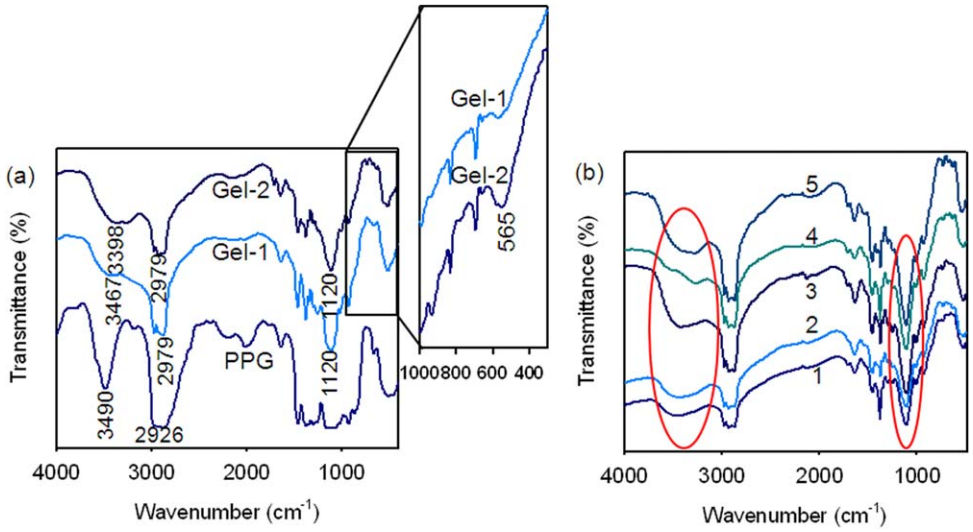

Figure 4. FT-IR spectra of (a) PPG, Gel-1, and Gel-2, and (b) Gel-2 composites: (1) **Gel-2**-Cu, (2) **Gel**−2-Fe, (3) **Gel-2**-Hg, (4) **Gel-2**-Ni, and (5) **Gel-2**-Pb. [Color figure can be viewed in the online issue, which is available at wileyonlinelibrary.com.]

shown in Figure 4. The broad adsorption bands at ∼3389 and ∼3467 cm^{-1} in PPG, **Gel-1**, and **Gel-2** indicate N–H stretching in phosphoramide groups. The band at 2979 cm^{-1} is because of the CH_2 stretching vibration. The bands at approximately 1120 and 1112 cm^{-1} are ascribed to the P=O wagging vibration; these peaks are because of the reaction of $POCl_3$. The adsorption peak at ∼565 cm^{-1} is attributed to P–S stretching, which indicates the reaction of $POCl_3$ with EDT during the synthesis of **Gel-2**. In the spectrum of PPG (Figure 2), the adsorption peak at ∼3490 cm^{-1} is attributed to the O–H and C–OH stretching modes, while the band at 2926 cm^{-1} is because of the CH_2 stretching vibration. Figure 4(b) shows the FT-IR spectra of **Gel-2**-Fe, **Gel-2**-Co, **Gel-2**-Ni, **Gel-2**-Cu, **Gel-2**-Hg, and **Gel-2**-Pb composites. The peak at ∼3398 cm^{-1} ascribed to N–H bending in phosphoramide groups shifts to 3318, 3274, 3430, 3459, 3482 cm^{-1} in the **Gel-2**-Fe, **Gel-2**-Co, **Gel-2**-Ni, **Gel-2**-Cu, **Gel-2**-Hg, and **Gel-2**-Pb composites, respectively, while that at ∼1120 cm^{-1}, which is attributed to the bending of P=O, shifts to 1110, 1110, 1110, 1110, and 1111 cm^{-1}, respectively. These shifts are attributed to the adsorption of the metal ions on the hydrogels.

As there are phosphorous frameworks in the hydrogels (**Gel-1** and **Gel-2**), ^{31}P NMR spectroscopy could be a good tool to figure out the structural characteristics. The ^{31}P spectra (Figure 5) show obvious phosphoryl signals at around δ-0.28 ppm, −10.8 ppm for **Gel-1**, δ 16.5, −9.7, −23.4 ppm for **Gel-2**, which indicated the typical phosphamide structure as the main crosslinking spot.

Thermogravimetric Analysis (TGA)

Typical Thermogravimetric Analysis (TGA) graphs of weight loss as a function of temperature for the hydrogels and metal-ion–chelated hydrogels are shown in Figure 6. The relative thermal stability of the different hydrogels was assessed by comparing the weight losses within 25–700°C with a heating rate of 10°C/min. It is evident that **Gel-1** has a better thermal stability at high temperature (say about 400°C), which was attributed to the decomposition of amino groups in the polymer. However, **Gel-2** begins to lose weight at ∼140°C most probably because of the presence of P–S and C–S backbones, which may degrade relatively more easily than P–N and C-N bonds. The weight losses of **Gel-1** and **Gel-2** were not complete because they contain phosphorus from $POCl_3$.

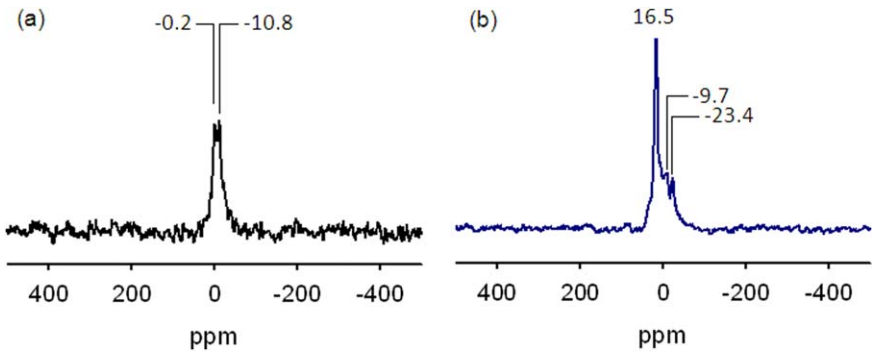

Figure 5. Solid-state ^{31}P NMR spectra of the hydrogels confirming the formation of $–CH_2–O–P(O)–(NH)_2–$ backbones: (a) **Gel-1** and (b) **Gel-2**. [Color figure can be viewed in the online issue, which is available at wileyonlinelibrary.com.]

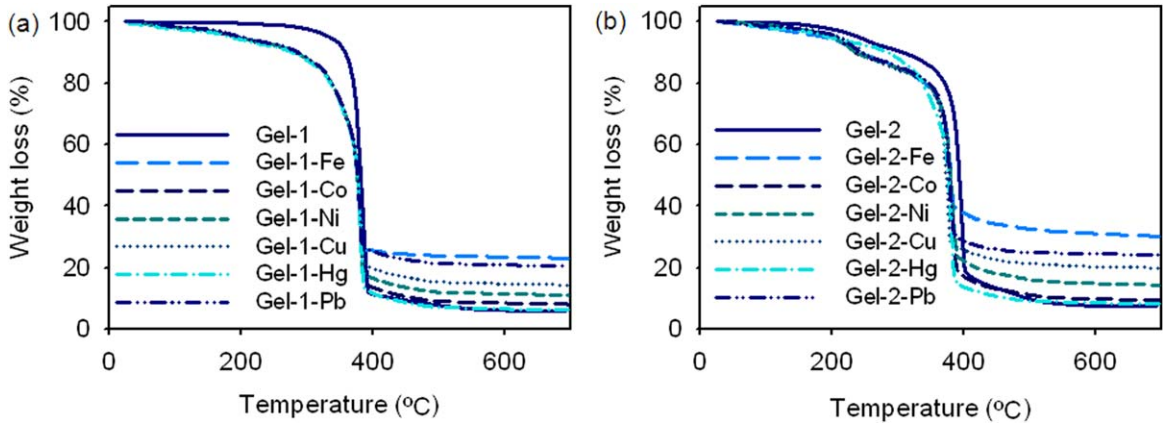

Figure 6. TGA results for **Gel-1** and **Gel-2** and their composites adsorbing various metal ions. [Color figure can be viewed in the online issue, which is available at wileyonlinelibrary.com.]

Figure 6(a) shows a typical TGA graph of weight loss as a function of temperature for **Gel-1** and its complexes: **Gel-1**-Fe, **Gel-1**-Ni, **Gel-1**-Co, **Gel-1**-Cu, **Gel-1**-Hg, and **Gel-1**-Pb. From this TGA data, it is evident that the complexes gradually lose weight up to 200°C and a sharp decrease occurs at approximately 350°C. This trend is also evident in Figure 5(b), which shows a typical TGA graph of weight loss as a function of temperature for **Gel-2** and its complexes: **Gel-2**-Fe, **Gel-2**-Ni, **Gel-2**-Co, **Gel-2**-Cu, **Gel-2**-Hg, and **Gel-2**-Pb. The sharp weight loss is observed up to 400°C. The overall weight remained after degradation at 700°C is 23.0%, 8.21%, 11.2%, 14.5%, 6.26%, and 20.6% for **Gel-1**-Fe, **Gel-1**-Ni, **Gel-1**-Co, **Gel-1**-Cu, **Gel-1**-Hg, and **Gel-1**-Pb, respectively, and 30.6%, 9.45%, 14.4%, 19.0%, 8.24%, and 24.3% for **Gel-2**-Fe, **Gel-2**-Ni, **Gel-2**-Co, **Gel-2**-Cu, **Gel-2**-Hg, and **Gel-2**-Pb, respectively. The species that are not decomposed above 500°C contain corresponding metal and oxide. Comparing TGA results of both **Gel-1** and **Gel-2** bearing various metal ions, the residual quantity decreases in order of Fe(III) > Pb(II) > Cu(II) > Ni(II) > Co(II) > Hg(II), indicating that the amounts of metal ions adsorbed are in the same order; this is consistent with the experimental results (*vide infra*).[28] The weight losses begun at relatively lower temperature for the hydrogels bearing various metal ions may be because of the loss of water coordinated to the corresponding metal ions.[29]

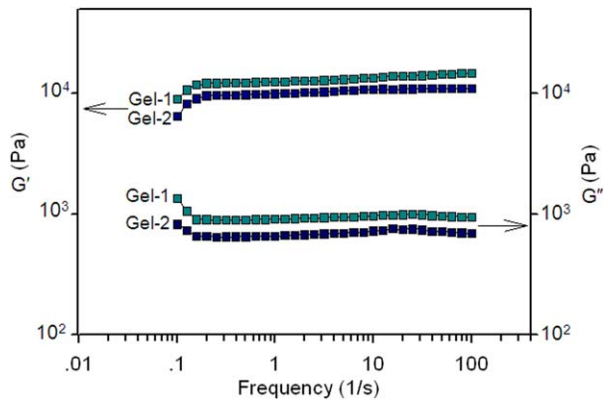

Figure 7. Storage (G') and loss moduli (G'') as a function of frequency of the hydrogels (**Gel-1** and **Gel-2**) measured at room temperature. [Color figure can be viewed in the online issue, which is available at wileyonlinelibrary.com.]

Rheological Measurements

One of the driving forces for constructing gels based on the condensation reaction in a one-pot process was the belief that controlled network formation would lead to an increase in mechanical properties. In Figure 7, the respective storage moduli (G') and loss moduli (G'') are shown as functions of angular frequency (0.1–100 rad s^{-1}). All samples have a single plateau region in their dynamic moduli. The G' values have a substantial elastic response and are always larger than the G'' values over the entire range of frequencies. The G' value decreases in accordance with a series: **Gel-1** > **Gel-2** and the same order is found in the G'' values for the two samples, indicating that the **Gel-1** bearing no sulfur atoms inside the network gets higher G' and G'' values. Wang and co-workers have shown that the gels with predominant performance should have radically cross-linked network structures.[30] The excellent properties of the

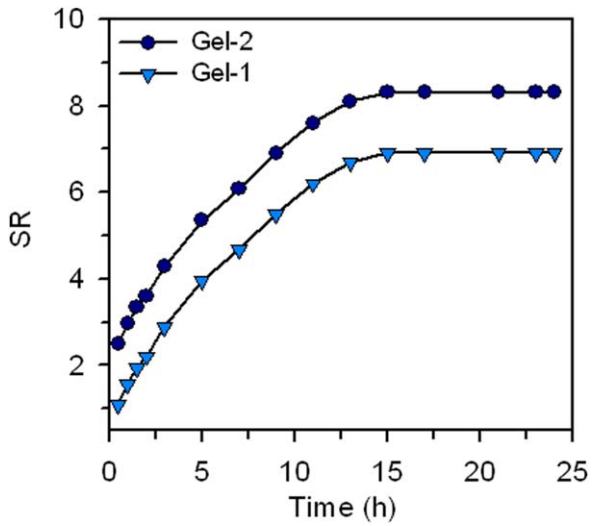

Figure 8. Swelling ratio (SR) of **Gel-1** and **Gel-2** according to time at room temperature. [Color figure can be viewed in the online issue, which is available at wileyonlinelibrary.com.]

Table I. Comparison of Various Metal Ions Uptake of **Gel-1** and **Gel-2**

	Metal-ion uptake (mg/g)							
Hydrogel	Fe(III)	Co(II)	Ni(II)	Cu(II)	Zn(II)	Cd(II)	Hg(II)	Pb(II)
Gel-1	291	63	115	154	203	225	53	252
Gel-2	329	108	143	190	241	272	82	294

hydrolges in the absence of any inorganic reinforcing materials may therefore be because of the controlled nature of the cross-linking reaction, leading to a more regular distribution of cross-link junctions, which improves the cross-linking degree.[31,32]

The cross-linking degree of the hydrogels was determined by the gel. The gel content of **Gel-1** (87.2%) is higher than **Gel-2** (85.8%), which means **Gel-1** has a higher cross-linking degree than **Gel-2**. Considering **Gel-1** contains phosphoramide groups from the reaction of modified phosphoryl oxychloride fragments with PDA inside the network and **Gel-2** bears these groups together with phosphorthiester groups, phosphorthiester groups contribute to lower the cross-linking degree of the hydrogel.

Swelling Measurements

The swelling values of **Gel-1** and **Gel-2** were obtained by immersing the hydrogels in sufficient volumes of distilled and deionized water at 25°C for 24 h and are shown in Figure 8. It is evident that the swelling increases during treatment and that the swelling rate of **Gel-2** is better than that of **Gel-1** as already visualized in Figure 2. The degree of hydration increases monotonously and then reaches asymptotic values at ~15 h. During the hydration procedure water molecules diffuse through the entire hydrogel matrix to render it soft and elastic. Subsequently, the swelling increases slowly until it reaches an asymptote at equilibrium.

Water molecules swell the polymer networks as they penetrate between the chains and breaks inter-chain secondary valence bonds via the formation of hydrogen bonds with the various groups such as phosphoramide, phosphorester, and phosporthioester (for **Gel-2**) within hydrogel matrix, and with hydroxyl, amine, and thiol (for **Gel-2**) groups in the periphery of the hydrogels. The presence of these hydrophilic groups is known to increase the hydrophilicity of the system and, consequently, increase the equilibrium swelling values of the samples in aqueous mediums[33]; this permits the polymer networks to expand to accommodate the influx of water via relaxation of the stresses produced by osmotic pressure.

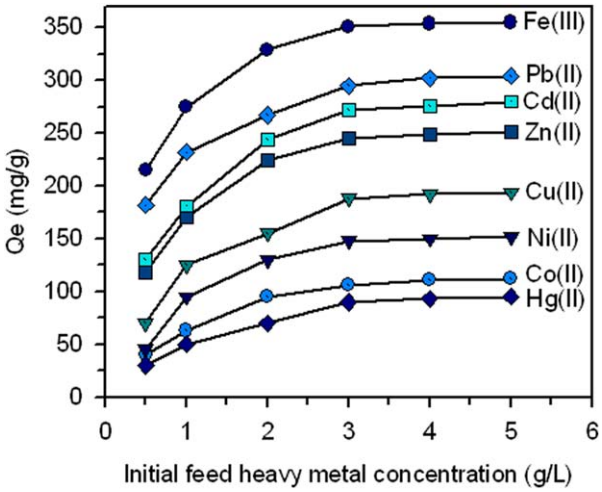

Figure 10. Effect of initial feed concentration of metal ions on the metal uptake capacity (Q_e) of **Gel-2**. [Color figure can be viewed in the online issue, which is available at wileyonlinelibrary.com.]

Adsorption of Metal Ions of the Hydrogels

Effect of the Type of Hydrogels. The adsorption of hydrogels with different compositions towards Fe (III), Co (II), Ni (II), Cu (II), Zn (II), Cd (II), Hg (II), and Pb (II) ions was investigated using the batch equilibration method. The amounts of metal ions adsorbed by the different hydrogels is summarized in

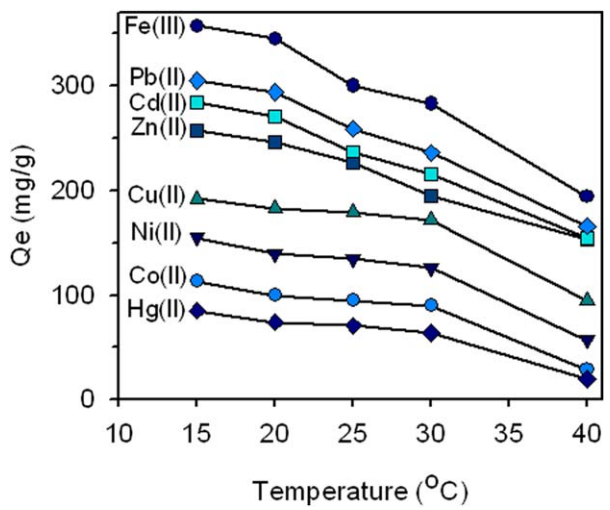

Figure 9. Effect of temperature on the metal uptake capacity of **Gel-2**. [Color figure can be viewed in the online issue, which is available at wileyonlinelibrary.com.]

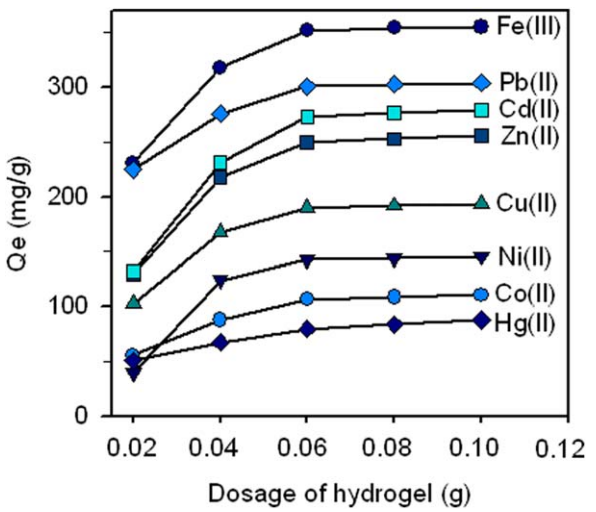

Figure 11. Effect of **Gel-2** dosage on the metal uptake capacity of Fe(III), Ni(II), Co(II), Cu(II), Zn(II), Cd(II), Hg(II), and Pb(II). [Color figure can be viewed in the online issue, which is available at wileyonlinelibrary.com.]

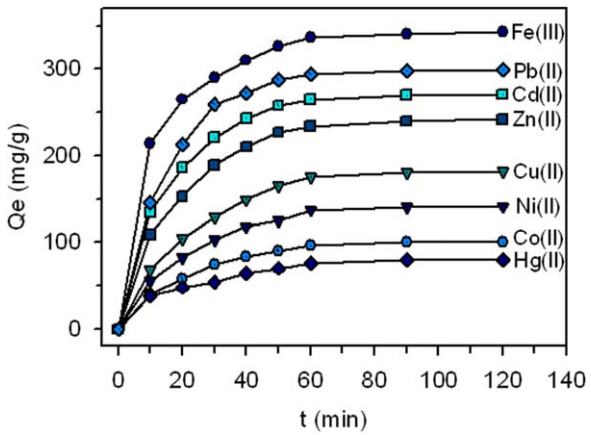

Figure 12. Metal-ion uptake of **Gel-2** at different adsorption times. [Color figure can be viewed in the online issue, which is available at wileyonlinelibrary.com.]

Table I. Both **Gel-1** and **Gel-2** show quite high metal adsorption capability ranging from 53 to 329 mg/g depending on the type of metal ions. **Gel-2** shows better adsorption capacity than **Gel-1** for all the metal ions tested in this study, demonstrating sulfur mediated functional groups are preferred for improving the swelling ratio of hydrogel and metal chelating capability. Table I also shows that the adsorption capability of **Gel-1** and **Gel-2** towards the metal ions decreases in the order of Fe(III) > Pb(II) > Cd(II) > Zn(II) > Cu(II) > Co(II) > Ni(II) > Hg(II). These results are in a very good agreement with the relative size and crystal field radii of the coordinated metal ions.[34]

Effect of Temperature. The effect of the temperature on metal-ions adsorption is investigated between 15°C and 40°C (Figure 9). The adsorption behavior of the hydrogels is greatly influenced by temperature. With increasing temperature, the capacity of the hydrogels for the adsorption of metal ions gradually decreases; this is because of the higher stability of the formed chelates at lower temperatures. The reduction in the adsorption capacity is relatively slow at the temperature lower than below 30°C; however, above 30°C, it decreased drastically from 283 to 194 mg/g, 236 to 166 mg/g, and 216 to 154 mg/g for Fe(III), Pb(II), and Cd(II), respectively. The results are of technical interest because these hydrogels exhibit higher efficiency at lower temperatures. At higher temperatures, metal ions have a higher velocity and activation energy.[35] Thus, it is easier for ions to escape from electrostatic affinity and chelation, which results in decrease of the adsorbed Ni(II), Co(II), Cu(II), and Hg(II).

Effect of Metal Concentration. The relationship between the nature of the hydrogel and its metal chelation behavior generally involves many possible interactions. Oxygen atoms in the hydroxyl group of the PPG, nitrogen atoms in the phophoramide and amino groups, and sulfur atoms in the phosphorthioester and thiol groups are responsible for the interactions of the metal ion with the hydrogel. For example, as mobile π-electrons are pulled strongly towards oxygen, the hydroxyl carbon is electron deficient and the hydroxyl oxygen is electron rich; therefore, the metal ions act as electron acceptors and coordinate to the donor oxygen of the hydroxyl group. The similar interactions with metal ions occur for the nitrogen and sulfur atoms.[36] The concentration of ions can be one of the important parameter that affects the adsorption ability of hydrogel. Figure 10 shows the adsorption capacity of **Gel-2** towards the metal ions with different initial concentrations ranging from 0.5 to 5 g/L. The adsorption capacity of metal ions increases slightly with increasing metal-ion concentration up to 3 mg/mL and then gradually plateaus. As the concentration of metal ions increases, the coordination number of the cations increases and more groups containing oxygen, nitrogen, and sulfur atoms are complexed. This phenomenon occurs with all metal ions used.[37] Giles et al.[38] divided the adsorption isotherms in solution into four types: S (shape), L (Langmuir), H (high affinity), and C (constant partition), respectively. From Figure 10, it is evident that the isotherm for the adsorption of metal ions by **Gel-2** is L-type, which means that many adsorption sites are distributed throughout the hydrogel. At higher concentrations, it is easier for metal ions to reach an adsorption site, while it becomes increasingly difficult for metal ions to reach the site with increased adsorption. There are two causes for the formation of L-type isotherms: (1) the arrangement of the adsorbate in the adsorbent is not vertical and (2) there are no competing adsorptions between the adsorbate and solvent

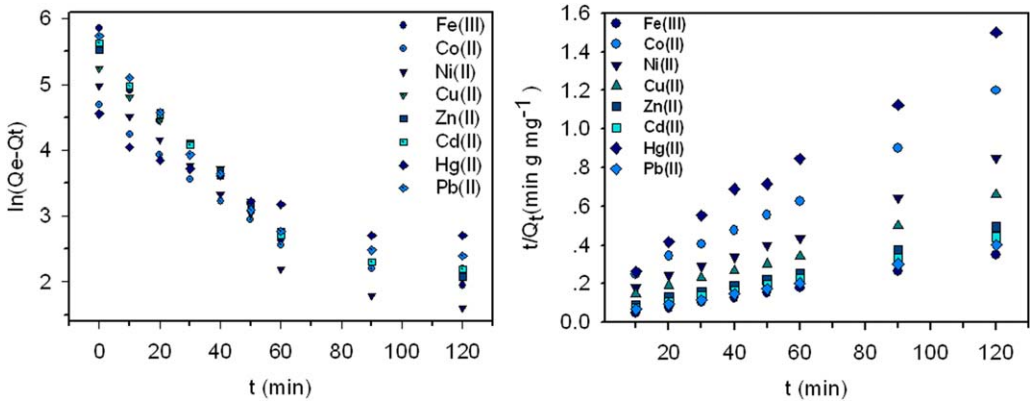

Figure 13. Linear simulations of the metal-ions adsorption kinetics of **Gel-2**: (a) pseudo–first-order model and (b) pseudo–second-order model. [Color figure can be viewed in the online issue, which is available at wileyonlinelibrary.com.]

Table II. Experimental Q_e Values and Kinetic Parameters of the Adsorption of **Gel-2** Based on Pseudo–First- and Pseudo–Second-Order Kinetic Models

		Pseudo-first-order model			Pseudo-second-order model		
Metal ions	Q_e,exp	Q_e,cal	k_1	R^2	Q_e,cal	k_2	R^2
Fe(III)	343	172	0.044	0.893	370	3.82×10^{-4}	0.999
Co(II)	100	73	0.042	0.880	118	4.86×10^{-4}	0.995
Ni(II)	141	103	0.045	0.919	167	3.33×10^{-4}	0.994
Cu(II)	182	138	0.048	0.921	217	2.38×10^{-4}	0.993
Zn(II)	245	158	0.050	0.906	278	2.65×10^{-4}	0.996
Cd(II)	271	156	0.049	0.872	303	3.14×10^{-4}	0.997
Hg(II)	80	67	0.015	0.897	93	5.72×10^{-4}	0.992
Pb(II)	299	156	0.048	0.830	334	3.18×10^{-4}	0.997

on the adsorbent surface.[38] In our system, the metal ions react with the active sites to form the most stable state. Once metal ions coordinate with the hydrogel, they lose their activity. Thus, an L-type isotherm was obtained.

Effect of Hydrogel Dosage. About 0.02, 0.04, 0.06, 0.08, and 0.10 g of **Gel-2** were placed into 2 mg/mL metal ion solutions at room temperature. After 24 h of oscillation adsorption, the ion removal rates were determined (Figure 11). The amounts of metal ions adsorbed (Q_e) increases monotonously at low hydrogel dosage (0.02–0.06 g); however, the rate of increase becomes limited at high dosage larger than 0.06 g. The increase of the metal-ion adsorption capacity according to hydrogel dosage is because the increased amount of hydrogel results in a greater number of surface adsorption sites, thereby enhancing the adsorption of various metal ions. At a dosage of 0.10 g, the adsorption capacity for Fe(III) was the highest (354 mg/g) followed by Pb(II) and Cd(II), whereas the removal of Hg(II) was the lowest. Therefore, in this experiment, the most suitable dosage of **Gel-2** was determined to be 0.06 g.

Effect of the Contact Time and Sorption Kinetics on Adsorption. To determine the effect of contact time on the adsorption of the metal ions at room temperature and to elucidate the adsorption kinetics of hydrogels, the metal-ion adsorption capacities were measured at specific time intervals and the results are shown in Figure 12. With increased contact time, the adsorption capacities towards the metal ions increased rapidly and then slowed; adsorption equilibrium was achieved within 120 min.

The kinetic models that were used to examine the mechanism of the adsorption process are based on the two most commonly used kinetic models: (1) The linear pseudo–first-order model [eq. (1)], and (2) the pseudo–second-order model [eq. (2)]

$$\ln (Q_e - Q_t) = -k_1 t + \ln Q_e \quad (3)$$

$$\frac{t}{Q_t} = \frac{t}{Q_e} + \frac{1}{k_2 Q_e^2} \quad (4)$$

where Q_e and Q_t are the amounts of metal ions adsorbed (mg/g) at equilibrium and at time t (min), respectively, k_1 (min^{-1}) and k_2 (g $mg^{-1}min^{-1}$) are the kinetics rate constants for the pseudo–first-order and pseudo–second-order models, respectively.

The kinetic parameters for the pseudo–first-order and pseudo–second-order models were obtained from linear plots of $\ln(Q_e - Q_t)$ versus t [Figure 13(a)] and t/Q_t versus t [Figure 13(b)], respectively. Table II lists the computed results of the first- and second-order kinetic models. Clearly, the correlation coefficients (i.e., R^2 in Table I) for the pseudo–second-order kinetic model are higher than those of the pseudo–first-order kinetic model, and the calculated data (Q_e,cal) from the pseudo–second-order kinetic model generally deviate less from the experimental data (Q_e,exp); this suggests that this adsorption system follows a pseudo–second-order kinetic adsorption process and that the adsorption is a chemical process.

CONCLUSIONS

New hydrogels with a microporous structure based on 6-functionalized PPG was synthesized in a one-pot protocol and characterized. Reaction of PPG with $POCl_3$, followed by with PDA (**Gel-1**) or with PDA and EDT (**Gel-2**) yielded structurally integral crosslink network. The swelling in water increased with the addition of EDT together with PDA, thus **Gel-2** showed higher swelling values in water than **Gel-1**. In addition **Gel-2** had a stronger capability for the adsorption of metal ions than **Gel-1** because of its higher swelling in water and chemical affinity towards metal ions induced by sulfur atoms in the matrix. We investigated the effects of temperature, concentration of metal ions, and hydrogel dosage on the adsorption capacities of the hydrogels toward various metal ions. At lower temperatures, higher hydrogel dosages, and higher concentrations of metal ions, the hydrogels exhibited a greater adsorption capacity. The capacity for the adsorption of the hydrogels was in order of Fe(III) > Pb(II) > Cd(II) > Zn(II) > Cu(II) > Ni(II) > Co(II) > Hg(II). The prepared hydrogel showed high thermal stability, which enables chelation at elevated temperatures. These results reveal the benefits of the new hydrogels for the treatment of industrial wastewater and other water polluted with metals.

ACKNOWLEDGMENTS

This work was supported by the Basic Science Research Program through the National Research Foundation of Korea funded by the Ministry of Education (2012R1A1A2041315) and the Fusion Research Program for Green Technologies through the National Research Foundation of Korea funded by the Ministry of

Education (2012M3C1A1054502). The authors also thank to BK21 PLUS Program for partial financial support.

REFERENCES

1. Karadag, E.; Uzum, O. B.; Saraydin, D.,; Guven, O. *Int. J. Pharm.* **2005**, *301*, 102.
2. Tang, Q. W.; Wu, J. H.; Lin, J. M.; Sun, H.; Ao, H. Y. *e-Polymers* **2008**, *1*, 21.
3. Saravanan, P.; Raju, M. P.; Alam, S. *Mater. Chem. Phys.* **2007**, *103*,278.
4. Wu, G.; Su, B.; Zhang, W. G.; Wang, C. T. *Mater. Chem. Phys.* **2008**, *107*, 364.
5. Yang, T.; Long, H.; Malkoch, M.; Gamstedt, E. K.; Berglund, L.; Hult, A. *J. Polym. Sci. A Polym. Chem.* **2011**, *49*, 4044.
6. Zhu, J. M. *Biomaterials* **2010**, *31*, 4639.
7. Lin, C. C.; Anseth, K. S. *Pharm. Res.* **2009**, *26*, 631.
8. Dijk, M. V.; Nostrum, C. F. V.; Hennink, W. E.; Rijkers, D. T. S.; Liskamp, R. M. *J. Biomacromolecules* **2010**, *11*, 1608.
9. Lee, S. H.; Lee, W. G.; Chung, B. G.; Park, J. H.; Khademhosseini, A. *Macromol. Rapid Commun.* **2009**, *30*, 1382.
10. Kloxin, A. M.; Benton, J. A.; Anseth, K. S. *Biomaterials* **2010**, *31*, 1.
11. Tyagi, P.; Li, Z.; Chancellor, M.; DeGroat, W. C.; Yoshimura, N.; Huang, L. *Pharm. Res.* **2004**, *21*, 832.
12. Rice, M. A.; Sanchez-Adams, J.; Anseth, K. S. *Biomacromolecules* **2006**, *7*, 1968.
13. Andreopoulos, F. M.; Persaud, I. *Biomaterials* **2006**, *27*, 2468.
14. Huang, Z.; Wu, Q.; Liu, S.; Liu, T.; Zhang, B. *Carbohydr. Polym.* **2013**, *97*, 496.
15. Vismara, E.; Melone, L.; Gastaldi, G.; Cosentino, C.; Torri, G. 2009, *J. Hazard. Mater.* **2009**, *170*, 798.
16. Cao, J.; Tan, Y. B.; Che, Y. J.; Xin,H. P. *Bioresour. Technol.* **2010**, *101*, 2558.
17. Juan, A. S.; Hlawaty, H.; Chaubet, F.; Letourneur, D.; Feldman, L. J. *J. Biomed. Mater. Res. A* **2007**, *82*, 354.
18. Tang, Q. W.; Sun, X. M.; Li, Q. H.; Wu, J. H.; Lin, J. M. *Sci. Technol. Adv. Mater.* **2009**, *10*, 015002.
19. Zhang, X. Z.; Wu, D. Q.; Chu, C. C. *Biomaterials* **2004**, *25*, 4719.
20. Wu, J. H.; Wei, Y. L.; Lin, J. M.; Lin, S. B. *Polymer* **2003**, *44*, 6513.
21. Delley, B. *J. Chem. Phys.* **2000**, *113*, 7756.
22. Perdew, J. P.; Wang, Y. *Phys. Rev. B* **1992**, *45*, 13244.
23. Delley, B. *New J. Chem.* **1992**, *16*, 1103.
24. Andzelm, J.; King-Smith, R. D.; Fitzgerald, G. *Chem. Phys. Lett.* **2001**, *335*, 321.
25. Arndt, K. F.; Schmidt, T.; Reichelt, R. *Polymer* **2001**, *42*, 6785.
26. Suzuki, M.; Hirasa, O. *Adv. Polym. Sci.* **1993**, *110*, 241.
27. Tezuka, Y.; Murakamia, Y.; Shiomib, T. *Polymer* **1998**, *39*, 2973.
28. Lee, W. F.; Chen, Y. C. *Eur. Polym. J.* **2005**, *41*, 1605.
29. Ali, A. E.; Shawky, H. A.; Abd El Rehim, H. A.; Hegazy, E. A. *Eur. Polym. J.* **2003**, *39*, 2337.
30. Malkoch, M.; Vestberg, R.; Gupta, N.; Mespouille, L.; Dubois,P.; Mason, A. F.; Hedrick, J. L.; Liao, Q.; Frank, C. W.; Kingsbury, K.; Hawker, C. *J. Chem. Commun.* **2006**, *26*, 2774.
31. Gibson, S. L.; Jones, R. L.; Washburn, N. R.; Horkay, F. *Macromolecules* **2005**, *38*, 2897.
32. Katime, I.; Rodríguez, E. *J. Macromol. Sci. A Pure Appl. Chem.* **2001**, *38*, 543.
33. Kandile, N. G.; Nasr, A. S. *Carbohydr. Polym.* **2011**, *85*, 120.
34. Shannon, R. D. *Acta Crystallogr. A.* **1976**, *32*, 751.
35. Chauhan, G. S.; Jaswal, S. C.; Verma, M. *Carbohydr. Polym.* **2006**, *66*, 435.
36. Tang, Q. W.; Wu, J. H.; Sun, H.; Fan, S. J.; Hu, D.; Lin, J. M. *Polym. Compos.* **2009**, *30*, 1183.
37. Khalil, M. I.; Farag, S. *J. Appl. Polym. Sci.* **1998**, *69*, 45.
38. Giles, C. H.; Smith, D.; Huitson, A. J. *Colloid Interface Sci.* **1974**, *47*, 755.